Journal of Instrumentation

SISSA

OPEN ACCESS

Sub-micron scale transverse electron beam size diagnostics methodology based on the analysis of optical transition radiation source distribution

To cite this article: A. Aryshev *et al* 2020 *JINST* **15** P01020

Published by IOP Publishing for Sissa Medialab

Received: *October 12, 2019*
Accepted: *December 8, 2019*
Published: *January 17, 2020*

Sub-micron scale transverse electron beam size diagnostics methodology based on the analysis of optical transition radiation source distribution

A. Aryshev,[a] **R. Ainsworth,**[b] **T. Aumeyr,**[b] **M. Bergamaschi,**[b] **S.T. Boogert,**[b] **P. Karataev,**[b,1] **R. Kieffer,**[c] **K. Kruchinin,**[b] **T. Lefevre,**[c] **S. Mazzoni,**[c] **L. Nevay,**[b] **N. Terunuma**[a] **and J. Urakawa**[a]

[a] *KEK: High Energy Accelerator Research Organization, 1-1 Oho, Tsukuba, Ibaraki 305-0801, Japan*
[b] *John Adams Institute at Royal Holloway, University of London, Egham, Surrey, TW20 0EX, U.K.*
[c] *CERN: European Organisation for Nuclear Research, CH-1211 Geneva 23, Switzerland*

E-mail: Pavel.Karataev@rhul.ac.uk

Abstract: Optical Transition Radiation (OTR) appearing when a charged particle crosses a boundary between two media with different dielectric properties has widely been used as a tool for transverse profile measurements of charged particle beams in numerous facilities worldwide. The resolution of the conventional monitors is defined by the dimensions of the Point Spread Function (PSF) distribution, i.e. the source distribution generated by a single electron and projected by an optical system onto a detector. The PSF form significantly depends on various parameters of the optical system like diffraction of the OTR tails, spherical and chromatic aberrations. The beam image is a convolution of the PSF with a transverse electron distribution in a beam. In our experiment we designed and built a system that can measure the transverse electron beam size through the analysis of the PSF distribution shape. In this paper we present the hardware, data analysis, calibration technique, a discussion on the main source of uncertainties and initial measurements of a micron-scale electron beam size with sub-micrometre resolution.

Keywords: Beam-line instrumentation (beam position and profile monitors; beam-intensity monitors; bunch length monitors); Instrumentation for particle accelerators and storage rings - high energy (linear accelerators, synchrotrons)

[1] Corresponding author.

https://doi.org/10.1088/1748-0221/15/01/P01020

2020 JINST 15 P01020

Contents

1 Introduction **1**
- 1.1 State-of-the-art in transverse electron beam size diagnostics in linear accelerators 2
- 1.2 Optical transition radiation diagnostics 2

2 Theoretical background **3**

3 Experimental setup **5**
- 3.1 Accelerator Test Facility (ATF/ATF2) 5
- 3.2 OTR experimental station 6
- 3.3 OTR image calibration 7

4 Optimisation of the OTR monitor and evaluation of uncertainties **8**
- 4.1 Image rotation 10
- 4.2 Optimisation of the longitudinal lens position 11
- 4.3 Beam size calibration procedure 11
- 4.4 Integration window and its position selection 12
- 4.5 Uncertainties 13

5 Beam size and emittance measurements **13**

6 Conclusion **15**

2020 JINST 15 P01020

1 Introduction

Nowadays accelerators are widely used in very different fields, covering a broad range of applications including both compact ones used for medical or industrial applications and large particle colliders used to study the properties of elementary particles and forces [1]. They require a full suite of diagnostics [2] to monitor and optimise the particle beam behaviour in an accelerator. Transverse beam size and emittance are the key parameters for optimal accelerator performance. In electron machines the beam size diagnostics are challenging because the transverse beam dimensions might reach sub-micrometer dimensions. To diagnose such beams with reasonable accuracy we must employ non-standard solutions going beyond the state-of-the-art to achieve the resolution of the equipment which is much smaller than the size of the beam.

The Accelerator Test Facility (ATF2) was built at KEK: High Energy Accelerator Research Organisation in Japan to demonstrate an ability to generate ultra-low emittance electron beam, that can be focused down to few tens of nanometres as needed for an International Linear Collider (ILC) [3, 4]. In ILC [5] the beam will be generated with a relatively large emittance by a photo-cathode RF gun, pre-accelerated to few GeV beam energy, cooled down in a damping ring, injected

in the main linac for final acceleration to extremely high energy and, then, squeezed down to a few nanometres at the interaction point. The ultimate performance of the collider depends directly on the measurement of low emittance beams from the exit of the damping ring to the interaction point. The ATF2 is a unique facility generating the beam with extremely small emittance that provides ideal experimental conditions in order to develop such challenging beam diagnostics.

1.1 State-of-the-art in transverse electron beam size diagnostics in linear accelerators

The resolution of optical diagnostics is usually defined by the diffraction limit, i.e. the optical wavelength and the angular aperture. One of the ways to break the diffraction limit is to use a relative phase of the wave. The state-of-the-art in transverse electron beam size diagnostics is based on Compton scattering interferometry [6], i.e. when a laser beam is split into two parts, which are then recombined to form interference fringes in the centre of the beam pipe. In case of a head-on recombination the standing wave periodicity of half a wavelength is produced. The electron beam is scanned across with the laser interference fringe pattern and the back-scattered Compton photons are registered downstream as a function for the fringe position. The visibility of the pattern is proportional to the electron beam size. In this case the resolution is defined by a fraction of the standing wave period which is much smaller than the laser wavelength. In [6] the authors demonstrated the beam size as small as 70 nm measured with laser interferometer. A laser-wire transverse beam size monitor is another internationally recognised candidate for micron-scale beam sizes for future accelerators [7, 8]. In this case a high quality high-power laser beam is focused down to a micrometre transverse dimensions with a sophisticated optics. Then the laser is scanned across the electron beam to measure its size with micrometre resolution. A beam size just a few micrometre wide was measured in [8]. Laser-based diagnostics are complex systems that require a team of expert to look after the high power laser and the alignment of optical system, in order to guarantee a reliable day-by-day operation and smooth maintenance. We have been investigating alternative method to measure micron-scale beam sizes in order to complement or replace laser wire scanners and laser interferometers.

1.2 Optical transition radiation diagnostics

Optical Transition Radiation (OTR) appears whenever a fast charged particle crosses a boundary between two media with different dielectric properties (e.g. a vacuum-metal interface). OTR is widely used to measure a few micrometre beam size which is just above the diffraction limit [9]. This is one of the best monitors which is simple in use and gives a two-dimensional beam profile in a single shot. The rms dimension of a so-called Point Spread Function (PSF) defines the resolution of conventional OTR monitors. In classical optics the PSF is an image generated by a point source emitting a spherical wave which is projected by an optical system on a detector. Due to the diffraction effect the image from a point object is no longer a point, but rather an extended distribution with dimensions defined by the wavelength and the optical system angular aperture. In case of OTR the PSF has a different definition. The OTR PSF is an image from a source induced by a single electron on a target surface and projected by an imaging optical system on a detector. As a matter of fact the source generated by a single electron is not a point but a distribution defined by the shape and dimensions of the charged particle electric field. In our previous work [10] we have represented the first observation of the OTR PSF and demonstrated that its vertical polarisation component has a two-lobe distribution. It was also very clear that the visibility of the pattern strongly depends

2020 JINST 15 P01020

on the electron beam size. In [11, 12] we have performed the first attempt to demonstrate the sensitivity of the OTR PSF to the beam size. In this paper we describe a transverse electron beam size monitor based on the analysis of shape of the OTR PSF including system configuration and laser alignment, detailed explanation of the data analysis, empirically found calibration procedure, and initial measurements of electron beam size. We shall also describe the detailed analysis and propagation of the uncertainties.

2 Theoretical background

Classical Optical Transition Radiation theory is based on the method of so-called pseudo-photons, i.e. when the relativistic electron field with characteristic radius of $\gamma\lambda/2\pi$ (where γ is the charged particle Lorentz factor and λ is the radiation wavelength) is represented as a superposition of virtual photons. The field is reflected off a flat metal-vacuum interface and propagates in the direction of specular reflection with characteristic opening angle of the order of γ^{-1} as is shown in 1.

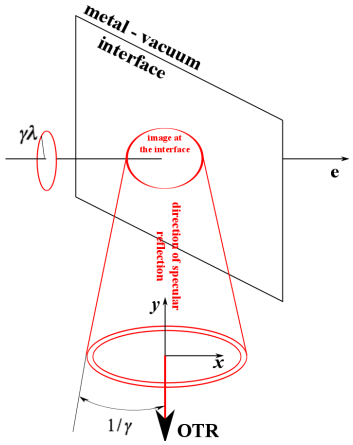

Figure 1. OTR generation geometry.

Consider a charge **e** moving in a vacuum with constant velocity **v** that crosses an interface between vacuum and a perfect conductor that results in generation of transition radiation. At ultra-relativistic energies ($\gamma \gg 1$) the large target tilt angles of the interface with respect to the particle trajectory do not change the OTR spectral-angular properties [15]. Therefore, mathematical treatment can be restricted to the normal incidence.

Assuming an optical system with an aberration-free lens with radius d located at a distance a from the source which, in this case, is the OTR screen and distance b from the image plane. The vertical polarisation component of the OTR field at an image point $P(\rho, \varphi)$ is given by [16]

$$E_y(P,\omega) = -\frac{2q\pi}{\beta c\lambda M}\sin\varphi\int_0^{\theta_{\text{lens}}} dt\,\frac{t^2}{t^2+(\beta\gamma)^{-2}}\left(\sqrt{1-t^2}+1\right)J_1(2\pi\rho t/\lambda M) \tag{2.1}$$

where $M = b/a$ is the lens magnification factor, λ is the wavelength, $\theta_{\text{lens}} = d/a$ is the angular acceptance of the lens. $\beta = v/c$ is the speed of the particle in units of the speed of light c, ϕ and $\rho = \sqrt{x^2+y^2}$ are the azimuthal angle and radius vector of the detector plane respectively with x

2020 JINST 15 P01020

and y being the cartesian coordinates of the detector (see figure 1). The intensity distribution in the image plane is given by

$$S(\rho, \omega) = \frac{c}{4\pi^2}|E_y|^2 \tag{2.2}$$

The OTR field in (2.1) is derived for a single particle and, thus, (2.2) represents a single particle intensity distribution (Point Spread Function, OTR PSF). If a bunch of particles is now considered, the resulting image is a convolution of the SPF with the transverse distribution of the bunch.

The distribution from (2.2) can be projected onto the y axis as

$$I(y, \omega) = \int S\left(\sqrt{x^2 + y^2}, \omega\right) \mathrm{d}x \tag{2.3}$$

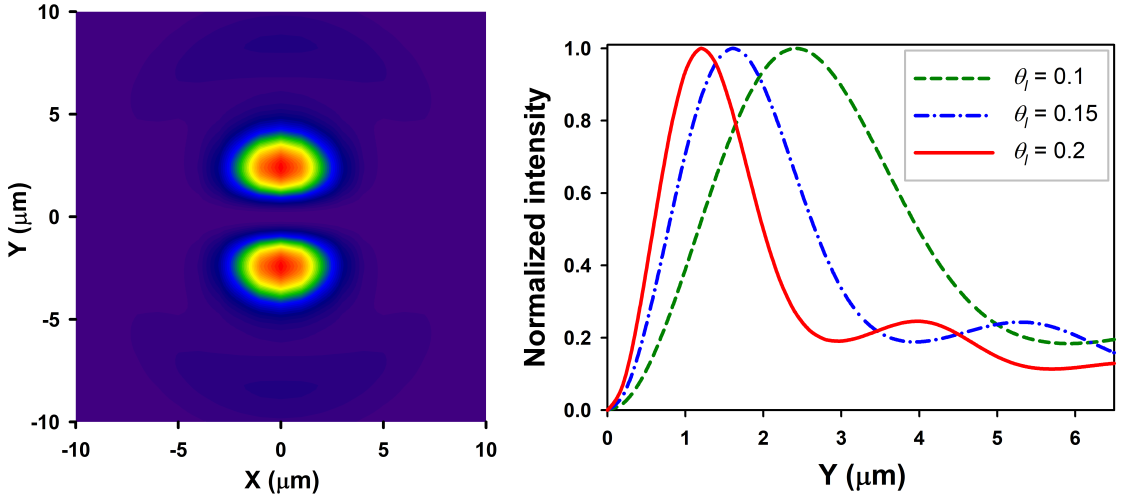

Figure 2. OTR PSF 2D image calculated using (2.2) and the angular acceptance $\theta_l = 0.1$ (left) and its projections (right) for different lens angular acceptances. Here $X = x/M$ and $Y = y/M$ are the coordinates of the target, x and y are the coordinates of the detector and M is the magnification factor. Parameters: $\beta\gamma = 2544$, $\lambda = 550$ nm.

Figure 2 shows the predicted OTR PSF for a particle with energy of 1.3 GeV and $\lambda = 550$ nm where $\theta_{\text{lens}} = 0.1$. The intensity at $y = 0$ is zero along the entire area of x. The resulting projection in the vertical direction is also shown for different θ_{lens}. One may see that the diffraction plays an important role in the width of the OTR PSF. If we have another particle which has a different transverse position, its image will have an offset. Considering a bunch of many particles will result in the fact that the minimum between two lobes will be smeared out. The degree of smoothing and, consequently, the sensitivity of the OTR PSF to the transverse beam size will depend on how wide the OTR PSF is. Therefore, an initially small angular acceptance will degrade the resolution of the method. The resolution limitations investigated using the ZEMAX software were well described by us in [17, 18]. It has been shown that the OTR PSF, as well as the method resolution, depend on spherical and chromatic aberrations. Nevertheless, if the optical system is well aligned, the OTR PSF depends on vertical beam size only. The effect of other parameters such as angular divergence or beam energy spread is negligibly small. The convolution of the OTR PSF with the transverse electron beam distribution is discussed later when we describe the calibration procedure.

2020 JINST 15 P01020

3 Experimental setup

3.1 Accelerator Test Facility (ATF/ATF2)

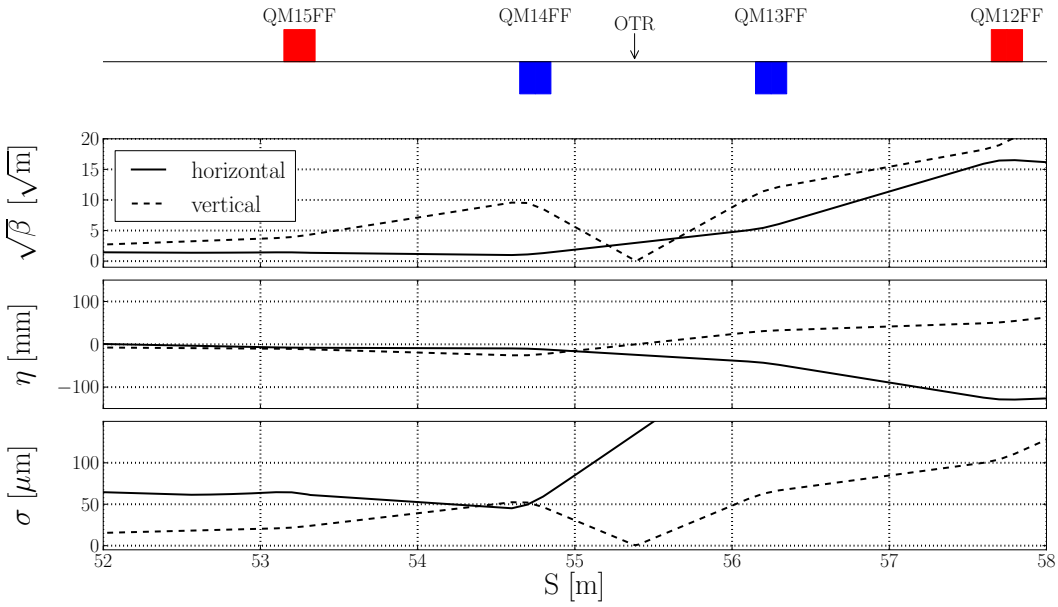

Figure 3. The beta function, dispersion and predicted electron beam size in the region of the OTR location (55.4 m).

Accelerator Test Facility (ATF) at KEK: High energy accelerator research organisation in Japan has been built in nineties to test advanced accelerator concepts for future electron-positron linear collider. It consists of a photo-cathode RF gun, 1.3 GeV S-band linear accelerator, damping ring and an extraction line. The ATF2 is an upgrade of the ATF extraction line with a final-focus test stand with the goal to focus the beam from the ATF damping ring down to the vertical beam size of 37 nm as well as to demonstrate its stability down to the nanometre level [3]. The OTR system is integrated into the laserwire system [8, 11, 12] with the aim to cross check the laser wire emittance measurement. Due to exactly the same location we anticipated linear correlation between OTR PSF and laser wire measurements unless resolution of either instrument counteracts it.

In order to generate sub-micrometre vertical beam sizes, a special beam optics was designed and used. Figure 3 shows the beta function $\beta_{x,y}$, the dispersion $\eta_{x,y}$ and the predicted electron beam size $\sigma_{x,y}$ calculated using MAD code. It can be seen that the beam is squeezed down in the vertical plane 55.4 m away from the point of extraction where the OTR monitor is located. The optics was different from the nominal ATF2 optics in which the local beam waist is located $\sim$ 20 cm further downstream. The dispersion is also set to be zero at the OTR monitor to minimise the beam size given by

$$\sigma = \sqrt{\beta\epsilon + \eta^2 \left(\frac{\Delta E}{E}\right)^2} \tag{3.1}$$

where β is the beta-function, ϵ is the physical beam emittance, η is the dispersion function and $\Delta E/E$ is the relative energy spread of the beam. Therefore, in the region of the OTR monitor, the beam

size is dominated by emittance term. If the ATF2 beam line is tuned very well and an emittance of 15 pm rad is achieved; therefore, a 0.5 μm beam size can be expected at OTR monitor location.

3.2 OTR experimental station

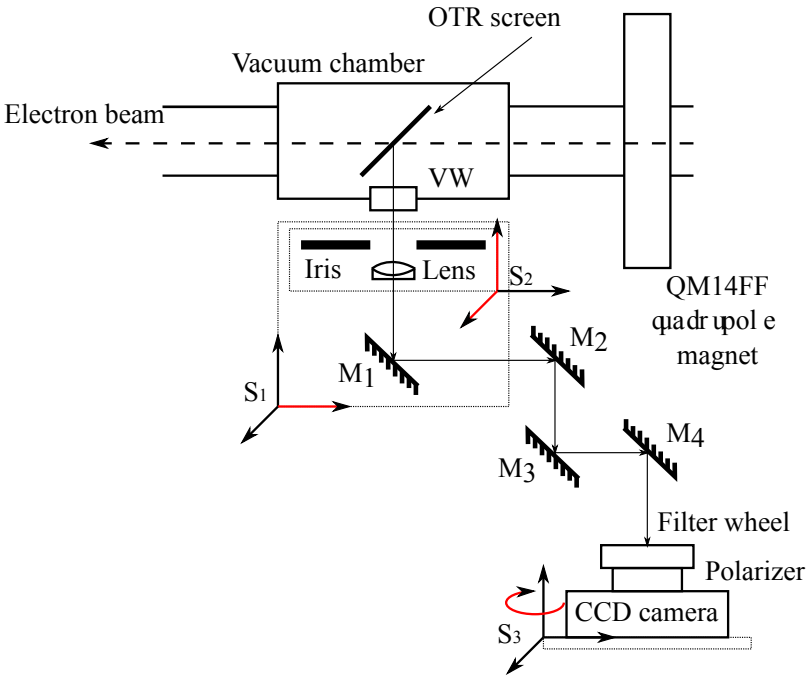

Figure 4. A schematic of the OTR setup in which the components are listed in table 1.

The experimental installation is schematically illustrated in figure 4. The OTR screen is a 30 × 30 × 0.3 mm aluminised silicon wafer tilted at 45° with respect to the electron beam trajectory. The target position and orientation angle was controlled using a four-dimensional vacuum manipulator (three translation and one rotation degrees of freedom) installed at the top of the vacuum chamber [8]. The OTR radiation propagates at 90° angle with respect to the electron beam, passes through the optical system consisting of a motorised iris, a lens, a periscope, an optical filter, a polariser and, finally, a CCD camera. The optical system components and their specifications are summarised in the table 1. The iris and the lens were mounted on the same board which can be moved using a stage (S_2) to adjust their centre position with respect to the radiation beam line. This board is also mounted on the stage (S_1) which along with S_2 allows 3D positioning of the lens. The optical filter followed by the polariser were attached to the CCD camera, which was mounted on a remotely controlled rotation stage (S_3). The whole setup was mounted on a breadboard and placed in a light protective enclosure.

To align the optical system a special alignment laser setup was used. A detailed description of the laser alignment is well described in [13, 14]. The laser stage located approximately 50 m upstream the OTR target consists of a CW He-Ne (Helium-Neon) laser with an output wavelength of 632.8 nm, a spatial filter, and a focusing lens enabling focusing the laser over a 100 m distance. A vacuum mirror is used to send the laser along the beam trajectory. Changing the distance between spatial filter and the focusing lens, one can focus the laser beam at each point of the setup. The

Table 1. The component list for the OTR setup.

Component	Component
VW	Vacuum window: CVI W2-PW-2050-UV-532-0-27
M_1	motorized aluminum mirror, ϕ = 50 mm
	mount: Thorlabs PT1-Z8, motor: Z625B
M_2-M_3	aluminium mirror, ϕ = 50 mm
M_4	aluminium mirror, ϕ = 75 mm
s_1	lens transverse stage: PI-410.2S
s_2	lens focus stage: Thorlabs PT1-Z8,
	motor Z625B lens vertical stage: Sigma-koki SGSP 60-10ZF
s_3	rotation stage: Suruga seiki K402-160-5
Lens	"CVI Laser Optics" cemented achromat, f=100 mm, ϕ=30 mm
Iris	Standa 8MID98-4-90
Filter wheel	Thorlabs FW102B
Polariser	Sigma-koki SPF-50C-32
CCD camera	SBIG-ST8300M based on Kodak KAF-8300 (monochrome)
	sensor with 5.4 μm pixel size, 3352×2532 pixel array
	and ~50% quantum efficiency

alignment better than $1/\gamma = 0.4$ mrad was achieved. The OTR screen inserted on the beam can reflect the laser along the optical path providing a reference trajectory to align the position and angles of all components of the optical system.

3.3 OTR image calibration

One crucial step in the monitor commissioning is the conversion of the measured distribution transverse coordinates from pixels to micrometres by means of well-defined calibration technique, which in turn determines the scale and dynamic range of the monitor system.

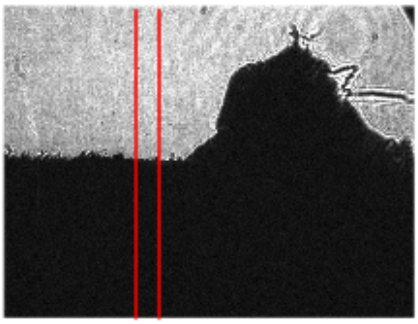

Figure 5. Image of the target edge.

2020 JINST 15 P01020

In order to convert the image size in pixels X_i^{pixel} into the image size in microns $X_i^{\mu m}$, the following procedure has been applied.

$$X_i^{\mu m} = \frac{X_i^{pixel} \cdot \text{binning} \cdot \text{pixel size}}{\text{magnification factor}} \tag{3.2}$$

Thus the magnification factor needs to be determined experimentally. The OTR screen edge reflecting the laser light can be observed by the CCD camera (see figure 5). The screen was gradually moved out of the vacuum chamber using the manipulator vertical translation mechanism. At each step the image of the OTR screen edge was recorded by the CCD. The position of the target was obtained from the manipulator motor encoder with $\pm 5\mu$m accuracy. A portion of the image shown with two vertical lines in figure 5 was chosen to produce the projections illustrated in figure 6 (left). The following function was used to fit the projected profile:

$$f(x) = a_0 + \frac{a_1}{1 + \exp\left(\frac{x - a_2}{a_3}\right)} \tag{3.3}$$

where a_0 is the vertical offset equivalent to the background intensity, a_1 is the amplitude, a_2 is the screen edge position and a_3 provides some information about the image focus, edge quality and the electron beam size. For each motor encoder position, the screen position, a_2, was found from the image and then plotted against the encoder position along with the linear fit shown in figure 6 (right). The magnification factor is the linear fit gradient multiplied by a single pixel size (5.4 μm in our case), which is $M = 20.4 \pm 0.5$ from figure 6 (right). Using eq. (3.2) now we can convert the image coordinates to microns in the target plane.

It is important to emphasise that the given procedure accuracy directly depends on a good lens longitudinal alignment and should be repeated every time the optical system is changed.

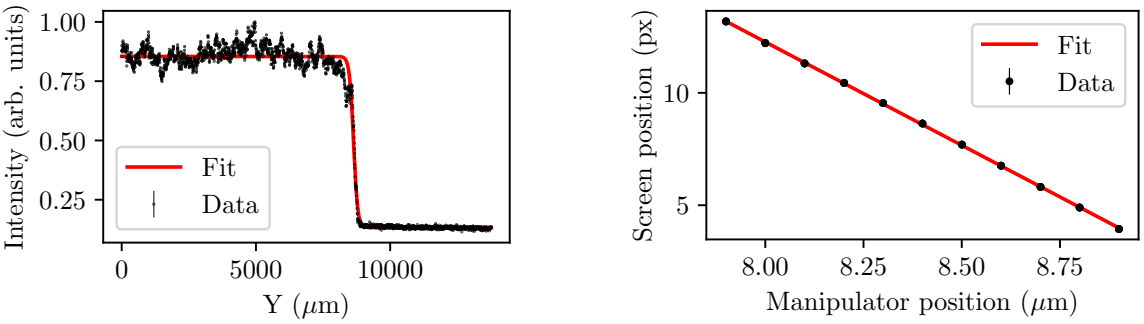

Figure 6. The effect of the beam size on the fit is shown (left) a long with an example calibration curve (right).

4 Optimisation of the OTR monitor and evaluation of uncertainties

Figure 7 shows an example OTR image. Its general appearance is similar to figure 2 in which the point spread function in the vertical direction is clearly visible from the two lobe distribution. However, the horizontal width is much larger due to the large beam size in the horizontal direction.

2020 JINST 15 P01020

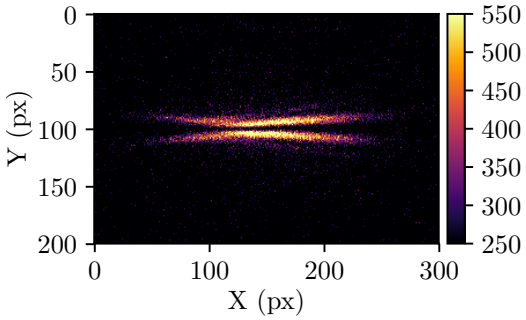

Figure 7. Typical OTR image.

A 'X' shape of the image is present due to the finite field of view of the optical system. The target is tilted at 45° with respect to the electron beam trajectory. However, the view port used to observe the OTR image is at 90°. Since our optical system is a microscope with large magnification factor, while the centre of the image is in the focus, the left and right parts of the beam in horizontal direction are out of focus. Such dilution of the OTR image degrades the resolution as the inter-peak distance increases, however, it does not effect the precision for the beam size diagnostics, since the beam size effect is still dominant here.

The horizontal projection is extracted by integrating the image along 'Y' axis. Employing symmetric Gaussian fit directly gives the horizontal RMS spot size in μm. An example is shown in figure 8 (left).The point spread function dimension in the horizontal direction is much smaller than the horizontal electron beam size. Therefore, the horizontal projection gives the horizontal electron beam profile. A Gaussian fit was used in figure 8 (left) which resulted in a beam size of 132 ± 0.3 μm, which is consistent with expectations from MAD [8, 12].

In order to analyse the vertical projection, a special fit function was proposed:

$$f(x) = a_0 + \frac{a_1 \left(a_4 + (x - a_3)^2\right)}{1 + (a_2(x - a_3))^4}. \tag{4.1}$$

where a_0 is the vertical offset of the distribution with respect to zero, a_1 is the amplitude of the distribution, a_2 is the smoothing parameter, a_3 is the horizontal offset of the central minimum with respect to zero and finally a_4 is the distribution width. This fit function is advantageous to the previously employed functions [12] as the distribution only has two maxima allowing the contrast ratio to be calculated analytically. An example vertical projection along with the fit is shown in figure 8 (right).

The contrast ratio of this distribution which is defined as the ratio of the central minimum intensity to the maximum intensity depends on the electron beam size. The ratio can be calculated analytically from the fit function parameters as

$$\frac{\mathrm{I_{min}}}{\mathrm{I_{max}}} = \frac{2a_2^2 a_4}{a_2^2 a_4 + \sqrt{1 + a_2^4 a_4^2}} \tag{4.2}$$

2020 JINST 15 P01020

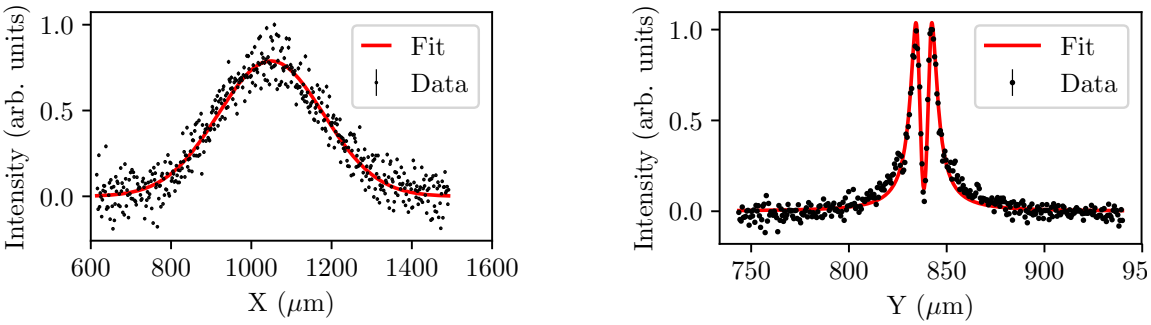

Figure 8. An example horizontal (left) and vertical (right) projection along with the associated fits.

For optical system optimisation the peak-to-peak (PTP) distance is used. The distance can also be calculated analytically from the fit function as

$$\mathrm{PTP} = \frac{2\sqrt{-a_2^2 a_4 + \sqrt{1 + a_2^4 a_4^2}}}{a_2} \tag{4.3}$$

One should point out that the image was measured with 550*nm* wavelength optical filter. However, the calibration of the image was performed with 632 nm He-Ne laser. In [12] we have demonstrated that the difference in wavelength of a 100 nm causes the change in PTP distance of about 1 % (thanks to the achromat lens), and, therefore the effect can be neglected.

The analysis of the beam extraction from the contrast ratio and calibration procedure are described in section 4.3.

4.1 Image rotation

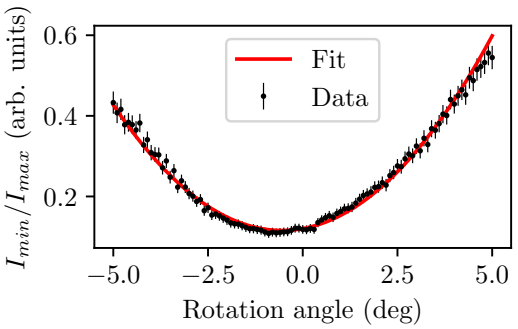

Figure 9. The contrast ratio as a function of image rotation angle.

During the initial commissioning of the monitor it is not clear what the orientation of the CCD camera is with respect to horizontal and vertical direction of the beam. Therefore, the image shown in figure 7 was digitally rotated to minimise the contrast ratio of the vertical projection. Figure 9 shows the contrast ratio as a function of the image tilt. A parabolic fit enables to extract the minimum ratio. For the current setup the minimum contrast ratio is obtained when the image is rotated by $-0.54°$. A similar tilt analysis has been performed for multiple images. All images share

2020 JINST 15 P01020

the same minimum rotation angle. Thus performing the rotation scan with one image is enough to determine the minimum for all other images in the data set. Nevertheless, when the entire system is upgraded or realigned the rotation scan has to be repeated.

4.2 Optimisation of the longitudinal lens position

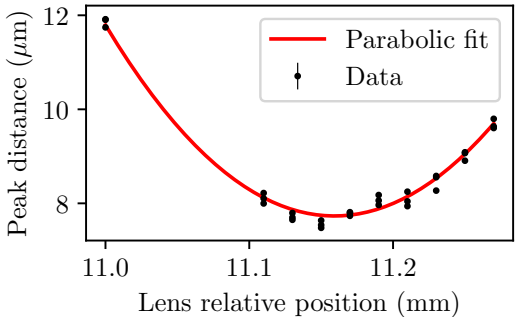

Figure 10. The effect of the PTP distance versus longitudinal lens position.

Due to a large magnification factor the image width in the detector plane is very sensitive to the longitudinal lens position. In [17–19] the authors used ZEMAX simulation software and analytical theory to demonstrate that the resolution for the beam size measurements directly depends on the OTR PSF width. An offset of a 100 μm can lead to significant resolution degradation. Therefore, a methodology of a beam-based longitudinal steering has been developed. When the lens is moving longitudinally the PTP distance changes. Figure 10 shows the PTP distance calculated from the fit using eq. (4.3) as a function of the S_2 stage longitudinal readout position. A parabolic fit enables us to find the minimal PTP distance that precisely corresponds to the best focus point which was used for beam size measurements.

A fine adjustment can be done by centring the minimum of the 'X' shaped image shown in figure 7. However, this shaped is only pronounced at 90 degrees observation angle with respect to the beam trajectory or smaller. At larger observation angles (e.g. 140 degrees) [20] the procedure shown in figure 10 should be used.

4.3 Beam size calibration procedure

To perform the calibration procedure a data set with varying vertical beam sizes is required. For each image, the PSF-like fit is used to extract the contrast ratio. The file with the smallest contrast ratio is then used for calibration as it is the closest fit to the original point spread function generated by a single electron. The fit curve for that file is then regenerated setting in (4.3) $a_0 = 0$ to remove any offset due to constant background and a_4 to zero in order to minimise the initial contrast ratio.

According to the principle of optics [21] for an idealised optical system, the PSF only depends on the incoherent source size. In accelerators the incoherent source size is defined by the transverse beam size. The influence of all other beam parameters is negligible and can be omitted.

2020 JINST 15 P01020

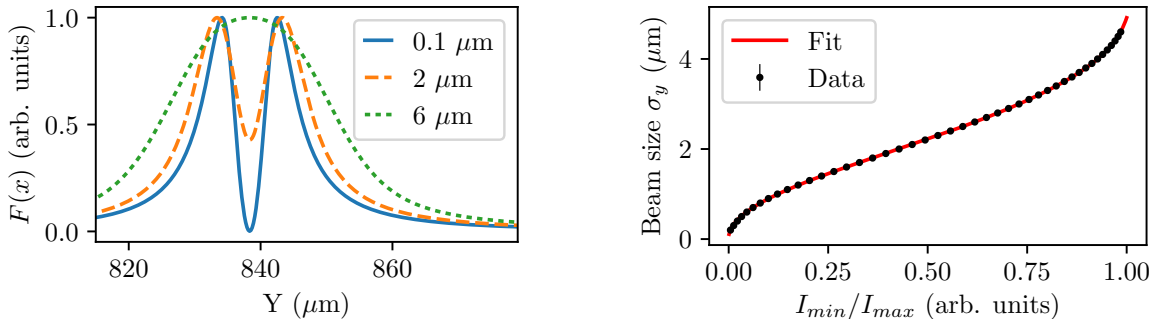

Figure 11. The effect of the beam size on the measured OTR PSF is shown (left) along with an example calibration curve (right).

Assuming a gaussian beam profile, the numerical convolution with the fit function is performed to take into account the effect of beam size as

$$F(x) = \frac{\sum_{i=1}^{N} f(x_i) \exp\left(\frac{-(x-x_i)^2}{2\sigma^2}\right)}{\sum_{i=1}^{N} \exp\left(\frac{-(x-x_i)^2}{2\sigma^2}\right)} \tag{4.4}$$

Here $f(x_i)$ is the measured intensity, x_i is the $x-$axis coordinate, and σ is the beam size. The left plot is figure 11 shows the effect of beam size on the PSF-like distribution. Increasing σ the contrast ratio slowly increases until the convoluted distribution reaches a pure Gaussian.

The calibration curve, i.e. $\sigma_y(x = I_{min}/I_{max})$, is illustrated in figure 11 (right). The following fit function is applied to obtain an analytical equation used to extract the beam size from calibration curve:

$$\sigma_y(x) = b_0 + \frac{1}{b_1}\left(-\ln\left(1 - \frac{x}{b_2}\right)\right)^{b_3} + b_4 x^{12} \tag{4.5}$$

The fit is also shown in the figure 11 (right, red). The resultant curve exhibits a symmetric nature. We expect larger beam size errors at each end of the curve. With the calibration now determined, it can be used to extract the vertical beam size for each image in the data set.

4.4 Integration window and its position selection

The choice of the integration window and its position affect the contrast ratio. Therefore, the calibration procedure has to be done every time the integration window is chosen, otherwise it might generate significant systematic deviation of the obtained beam size from a real value. The size of the integration window is also very important because together with useful signal we accumulate electronic noise in pixels and acquisition system of the CCD camera. To take that into account we developed a procedure enabling us to choose a range of integration windows and keep it during the beam size and emittance measurements.

Figure 12 (left) shows how the change of the gap size affect the contrast ratio. At small gap sizes, the quality of the fit produces a contrast ratio with large uncertainty due to very low number of photons. At very large gap size, a large amount of extra noise is included leading to an artificially

2020 JINST 15 P01020

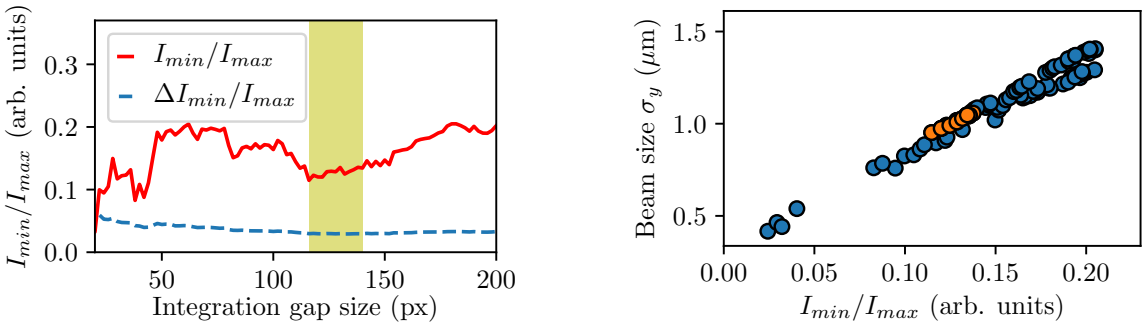

Figure 12. The contrast ratio and its error as a function of gap size (left). The correlation between contrast ratio and calibrated beam size for each gap size (right). The red dots represent the densest correlated region. This region is represented on the left plot as the highlight area.

high contrast ratio. In order to choose the correct region, the correlation of contrast ratio to beam size is used, as shown in figure 12 (right). The correct region for the gap size was chosen to be where the correlation has the densest number of points. This range does not exceed 5% of the mean value. In figure 12 (left) this is shown as a shadowed region and in figure 12 (right) as red points.

4.5 Uncertainties

The beam size measurements are single-shot. The uncertainty in this case is defined by pixel-by-pixel signal fluctuations of the CCD camera. Those fluctuations are well illustrated in figures 7 and 8. The numerical fits using eqs. (4.1) and (4.5) were performed using the Levenberg-Marquardt method to calculate the best parameters which minimised the weighted mean squared deviation of the experimental data and the best nonlinear fit function was used. The uncertainty of each parameter was then found by square-rooting the diagonal of the covariance matrix.

The uncertainty in the contrast ratio presented by eq. (4.2) was then found using the following propagation formula:

$$\Delta_{I_{\min}/I_{\max}} = \sqrt{\left(\frac{d}{da_2}\left(\frac{I_{\min}}{I_{\max}}\right)\right)^2 \cdot \Delta a_2^2 + \left(\frac{d}{da_4}\left(\frac{I_{\min}}{I_{\max}}\right)\right)^2 \cdot \Delta a_4^2} \tag{4.6}$$

where a_2 and a_4 are the free parameters of the fit function eq. (4.1), and Δa_2 and Δa_4 are their uncertainties from the fit procedure.

While the beam size cannot be extracted directly from the fit as in the case for the horizontal projection, the beam size is strongly dependent of the contrast ratio. In order to convert the contrast ratio to beam size, a self calibration procedure has been introduced in section 4.3. The uncertainty of the beam size obtained from eq. (4.5) is evaluated as

$$\Delta\sigma = \sqrt{\sum_{i=0}^{4}\left(\frac{d\sigma}{da_i}\right)^2 \cdot \Delta a_i^2 + \left(\frac{d\sigma}{dx}\right)^2 \cdot \Delta^2_{I_{\min}/I_{\max}}} \tag{4.7}$$

5 Beam size and emittance measurements

Initially the accelerator was carefully tuned to minimise the background levels and provide a stable working regime during the data taking. The longitudinal position of the focusing lens was adjusted to

2020 JINST 15 P01020

minimise the PTP distance of the OTR PSF as described in section 4.2 and the centre the 'X'-shaped image was adjusted. After that, the monitor was ready to perform beam size measurements.

We employed a single bunch mode, with repetition rate of 3.12 Hz and the bunch charge of ~ 1 nC. A quadrupole scan was then performed in which the current of the QM14FF quadrupole magnet was changed in the range from -88 A to -97 A in steps of 1 A. For each value of the quadrupole current, three OTR images were taken in order to reduce the effect of statistical fluctuations. Figure 13 shows the measured horizontal and vertical beam sizes at each current. It can be seen that the horizontal beam size remains roughly constant at around ~ 145 μm as desired while the beam size in the vertical direction shows a hyperbolic dependence with a minimum beam size of 0.91 ± 0.05 μm.

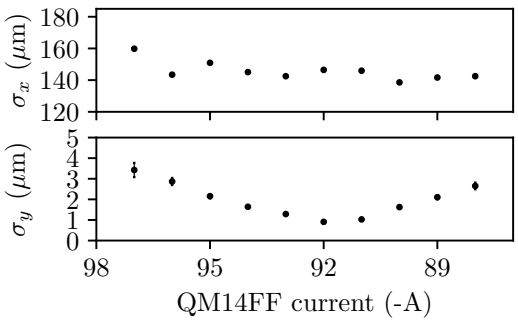

Figure 13. The measured horizontal (left) and vertical (right) electron beam sizes measured by the OTR system using QM14FF quadrupole at different currents.

The emittance can be found by measuring the σ-matrix.

$$\sigma = \begin{pmatrix} \sigma_y^2 & \sigma_{yy'} \\ \sigma_{yy'} & \sigma_{y'}^2 \end{pmatrix} = \epsilon_y \begin{pmatrix} \beta_y & -\alpha_y \\ -\alpha_y & \gamma_y \end{pmatrix} \tag{5.1}$$

The rms beam size $\sigma_y^2(s_2)$ at some distance downstream the quadrupole is related to the rms beam size at the quadrupole $\sigma_y^2(s_1)$ using the thick lens approach as

$$\sigma_y^2(s_2) = \sigma_y^2(s_1)\left(m_{11} + \frac{\sigma_{yy'}(s_1)}{\sigma_y^2(s_1)} m_{12}\right)^2 + \frac{\epsilon_y^2}{\sigma_y^2(s_1)} m_{12}^2 \tag{5.2}$$

where m_{ij} are the elements of the transfer matrix. For a focusing quadrupole the transfer matrix elements are defined as

$$m_{11} = \cos\sqrt{K} l_q - L\sqrt{K}\sin\sqrt{K} l_q, \quad m_{12} = \frac{1}{\sqrt{K}}\sin\sqrt{K} l_q + L\cos\sqrt{K} l_q \tag{5.3}$$

where l_q is the effective length of the quadrupole, K is the quadrupole field strength, and L is the distance between the quadrupole and the OTR screen. By making the following substitution

$$a = \sigma_y^2(s_1), \quad b = \frac{\sigma_{yy'}(s_1)}{\sigma_y^2(s_1)}, \quad c = \frac{\epsilon_y^2}{\sigma_y^2(s_1)} \tag{5.4}$$

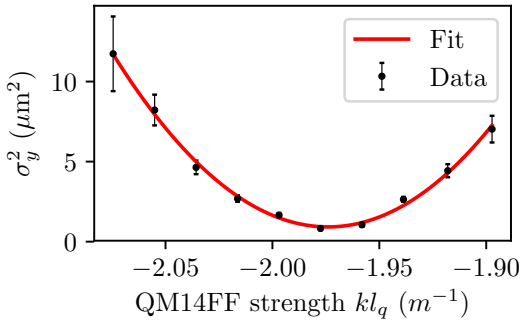

Figure 14. The measured beam size squared as a function of effective quad strength. The red line represents the parabolic fit used to extract the emittance.

we obtain parabolic fit function:

$$\sigma_y^2(s_2) = a(m_{11} + bm_{12})^2 + cm_{12}^2 \tag{5.5}$$

Thus, the emittance is $\epsilon = \sqrt{ac}$. From the data and the fit in figure 14, the emittance was found to be 59.3± 4.2 pm rad. The emittance was consistent with the laser-wire measurements [8]. The emittance was also measured the following shift using the multiOTR [23] and found to be 23 pm rad; however, this was measured after a series of beam tuning routines were performed and thus, a smaller emittance was expected.

6 Conclusion

In this paper we present a detailed step-by-step methodology for beam size measurements using optical transition radiation point spread function technique including detailed design, alignment and tuning procedure. Beam size as small as 0.91 ± 0.05 μm was measured. We have also demonstrated extremely low emittance which was consistent with laser wire measurements. Current methodology has been applied to verify e-beam optics at ATF2 facility for laser-wire experiment [8] and calibrate non-invasive Optical Diffraction Radiation monitor [20]. In order to improve the beam size measurement technique additional efforts toward the optimisation of the optical system, e.g. spherical and chromatic aberrations, has to be invested.

References

[1] A. Sessler and E. Wilson, *Engines of discovery*, World Scientific, Singapore (2007).

[2] M.G. Minty and F. Zimmermann, *Measurement and control of charged particle beams*, Springer, Germany (2003).

[3] ATF2 collaboration, *Experimental validation of a novel compact focusing scheme for future energy-frontier linear lepton colliders*, *Phys. Rev. Lett.* **112** (2014) 034802.

[4] P. Bambade et al., *Present status and first results of the final focus beam line at the KEK accelerator test facility*, *Phys. Rev. ST Accel. Beams* **13** (2010) 042801 [arXiv:1207.1334].

[5] T. Behnke et al. eds., *International Linear Collider — technical design report*, arXiv:1306.6327.

2020 JINST 15 P01020

[6] V. Balakin et al., *Focusing of submicron beams for TeV scale e^+e^- linear colliders*, *Phys. Rev. Lett.* **74** (1995) 2479.

[7] S.T. Boogert et al., *Micron-scale laser-wire scanner for the KEK accelerator test facility extraction line*, *Phys. Rev. ST Accel. Beams* **13** (2010) 122801.

[8] L.J. Nevay et al., *Laserwire at the accelerator test facility* 2 *with sub-micrometre resolution*, *Phys. Rev. ST Accel. Beams* **17** (2014) 072802 [arXiv:1404.0294].

[9] M. Ross et al., *A very high resolution optical transition radiation beam profile monitor*, *AIP Conf. Proc.* **648** (2002) 237

[10] P. Karataev, A. Aryshev, S. Boogert, D. Howell, N. Terunuma and J. Urakawa, *First observation of the point spread function of optical transition radiation*, *Phys. Rev. Lett.* **107** (2011) 174801.

[11] A. Aryshev et al., *A novel method for sub-micrometer transverse electron beam size measurements using optical transition radiation*, *J. Phys. Conf. Ser.* **236** (2010) 012008.

[12] K. Kruchinin et al., *Sub-micrometer transverse beam size diagnostics using optical transition radiation*, *J. Phys. Conf. Ser.* **517** (2014) 012011.

[13] P. Karataev et al., *Beam-size measurement with optical diffraction radiation at KEK accelerator test facility*, *Phys. Rev. Lett.* **93** (2004) 244802.

[14] P. Karataev et al., *Observation of optical diffraction radiation from a slit target at KEK accelerator test facility*, *Nucl. Instrum. Meth.* **B 227** (2005) 158.

[15] A. Potylitsyn, *Transition radiation and diffraction radiation. Similarities and differences*, *Nucl. Instrum. Meth.* **B 145** (1998) 169.

[16] M. Castellano and V.A. Verzilov, *Spatial resolution in optical transition radiation (OTR) beam diagnostics*, *Phys. Rev. ST Accel. Beams* **1** (1998) 062801.

[17] B. Bolzon et al., *Very high resolution optical transition radiation imaging system: comparison between simulation and experiment*, *Phys. Rev. ST Accel. Beams* **18** (2015) 082803.

[18] T. Aumeyr et al., *Advanced simulations of optical transition and diffraction radiation*, *Phys. Rev. ST Accel. Beams* **18** (2015) 042801.

[19] L.G. Sukhikh, G. Kube and A.P. Potylitsyn, *Simulation of transition radiation based beam imaging from tilted targets*, *Phys. Rev. Accel. Beams* **20** (2017) 032802.

[20] M. Bergamaschi et al., *Non invasive micron-scale particle beam size measurement using optical diffraction radiation in the ultra violet wavelength range*, *Phys. Rev. Appl.* accepted, (2019).

[21] M. Born and E. Wolf, *Principles of optics*, 7th edition, Cambridge University Press, Cambridge, U.K. (1999).

[22] G. Cowan, *Statistical data analysis*, Clarendon Press, Oxford, U.K. (1998).

[23] C. Blanch Gutierrez et al., *Multi optical transition radiation system for ATF*2, in *Proceedings of DIPAC'*2011, Hamburg, Germany (2011).

2020 JINST 15 P01020